Irreversible phase transformation in a CoCrFeMnNi high entropy alloy under hydrostatic compression

E-Wen Huang[a,b,*], Chih-Ming Lin[c,**], Jayant Jain[d], Sean R. Shieh[e], Ching-Pao Wang[e], Yu-Chun Chuang[f], Yen-Fa Liao[f], Dong-Zhou Zhang[g], Tony Huang[h], Tu-Ngoc Lam[a], Wanchuck Woo[i], Soo Yeol Lee[j]

[a] Department of Materials Science and Engineering, National Chiao Tung University, 1001 University Road, Hsinchu, 30010, Taiwan
[b] Materials and Chemistry Laboratoires, Industrial Technology Research Institute, Hsinchu City, 300, Taiwan
[c] Department of Physics, National Tsing Hua University, Hsinchu, 30013, Taiwan
[d] Department of Applied Mechanics, Indian Institute of Technology, New Delhi, India
[e] Department of Earth Sciences, University of Western Ontario, London, ON, N6A 5B7, Canada
[f] National Synchrotron Radiation Research Center, Hsinchu, 30076, Taiwan
[g] GeoSoilEnviroCARS, Argonne National Laboratory, United States
[h] Department of Earth Sciences, National Cheng Kung University, Tainan, 701, Taiwan
[i] Neutron Science Center, Korea Atomic Energy Research Institute, Daejeon, 34057, Republic of Korea
[j] Department of Materials Science and Engineering, Chungnam National University, Daejeon, 34134, Republic of Korea

ARTICLE INFO

ABSTRACT

An equal-molar CoCrFeMnNi, face-centered-cubic high-entropy alloy system is investigated using *in-situ* angular-dispersive X-ray diffraction under hydrostatic compression up to 20 GPa *via* diamond anvil cell. The evolutions of multiple diffraction peaks are collected simultaneously to elucidate the phase stability field. The results indicated that an irreversible phase transformation had occurred in the high entropy alloy upon decompression to ambient pressure. A reference material (n-type silicon-doped gallium arsenide) was investigated following the same protocol to demonstrate the different deformation mechanisms. It is suggested that the atomic bonding characteristics on the phase stability may play an important role in the high entropy alloys.

1. Introduction

Superior fracture-resistant properties of equiatomic, face-centered cubic (fcc), CoCrFeMnNi [1] and CrCoNi [2] at cryogenic temperatures have drawn great attention in the category of high-entropy alloys (HEAs) and the medium-entropy alloys, respectively. To understand the underneath deformation mechanisms in the HEAs, Huang et al.'s [3] *ab initio* calculations reported that the temperature-dependent plasticity of CoCrFeMnNi HEA is superior due to the activation of its different deformation modes at low temperature. Moreover, they proposed three deformation regimes based on the deformation temperature as i) from room to high temperature, dislocation glide *i.e.* the slip as the main event; (ii) from room temperature to 77 K, both slip and twinning (twinning induced plasticity (TWIP) effect) are predicted, and (iii) below 77 K, a possible transition from TWIP + Slip towards transformation induced plasticity (*i.e.* TRIP) effect. Recently, Zhang et al. [4] reported the presence of stacking fault and twin on CrCoNi using *in-situ*

electron microscopy. Their results revealed the distinct stacking-fault and twin evolutions subjected to plastic deformation. Furthermore, their first-principles calculations exhibited that the fcc HEAs inherently have negative stacking faults energies (SFEs) which could be the origin of their superior plasticity at low temperatures [5].

The underneath mechanical mechanisms of this CoCrFeMnNi HEA have been reported extensively [1,6–14]. In summary, the complex microstructure evolutions and metastable phase transitions subjected to the deformation are frequently observed in the medium and HEAs.

However, the thermodynamics of the HEA systems is still not fully understood yet and there is a strong need to quantify both the applied-stress and the environmental-temperature effects. Since the stable phase (s) always processes toward the lowest Gibbs free energy, the phase transformation tendency can be evaluated from the sign of $\Delta G(P, T)$ in the following thermodynamics relation.

* Corresponding author at: Department of Materials Science and Engineering, National Chiao Tung University, 1001 University Road, Hsinchu, 30010, Taiwan.
** Corresponding author.
E-mail addresses: EwenHUANG@nctu.edu.tw (E.-W. Huang), cmlin@mail.nd.nthu.edu.tw (C.-M. Lin).
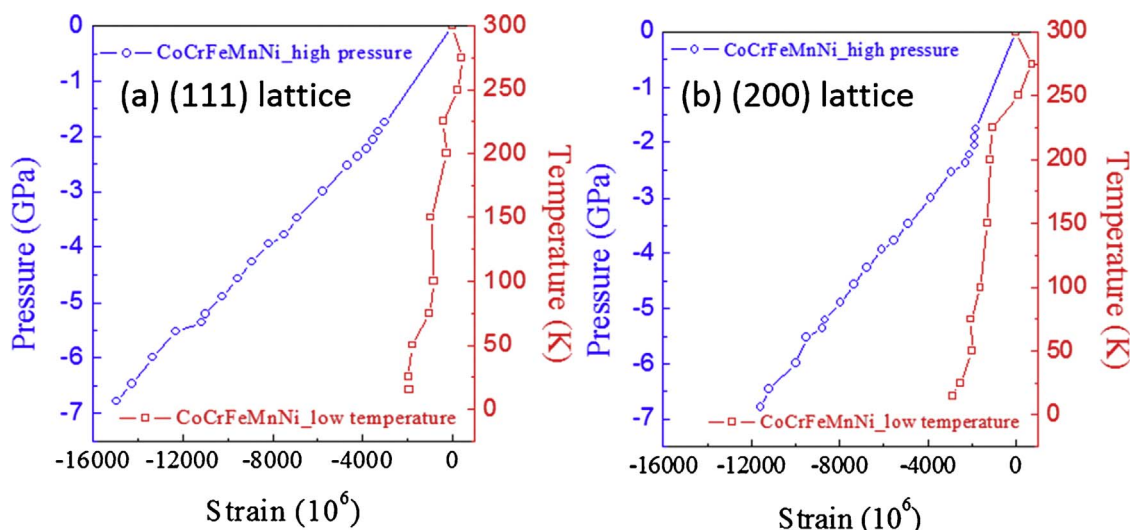
Fig. 1. Variation of lattice strains subjected to hydrostatic compression (in blue/left y-axis) and temperature (in red/right y-axis) for (a) (1 1 1) lattice and (b) (2 0 0) lattice of the CoCrFeMnNi HEA.

$$\Delta G(P, T) = \Delta G(P_0, T_0) - \int_{T_0}^{T} \Delta S(P_0, T)dT + \int_{P_0}^{P} \Delta V(T_0, P)dP \qquad (1)$$

Where ΔG, ΔS, and ΔV are changes in the Gibbs free energy, entropy, and volume, respectively, at a given pressure (P) and temperature (T). P_0 is usually 1 bar, T_0 is frequently considered as 0 K for theoretical calculations or 298 K for experimental measurements.

So far, most of the plasticity studies of the HEAs quantify the onset temperatures of different deformation modes. Some theoretical calculations are based on the assumptions at the 0 K environments, which may lead to possibilities of missing high-pressure phase (s) and/or introducing metastable phase (s).

At present, there are several experimental studies that examine the behavior of HEAs under high pressure hydrostatic environment [13–16]. For instance, the work of Zhang et al. [15] on Ni-based high entropy solid solution alloys (NiCoCr, NiCoCrFe, and NiCoCrFePd) showed a pressure-induced phase transition from the fcc to the hexagonal close-packed (hcp) structure. The results suggested that Ni-CoCrFe solid solution alloy starts to transform at 13.5 GPa. They also emphasized that phase transition is very sluggish which even does not get completed until 40 GPa. Their *ab initio* Gibbs free energy calculations demonstrated that the energy differences between the fcc and hcp phases for the three alloys are very small. In addition, Zhang et al. [13] and Tracy et al. [14] have recently demonstrated the polymorphism and high pressure phase behavior in the CoCrFeMnNi HEA system. On the other hand, the work of Yu et al. [6] on CoCrFeCuNi and CoCrFeMnNi (prepared by mechanical alloying and high pressure sintering with a grain size of about 100 nm) HEAs suggested that there is no obvious transformation in the structures even after subjecting to a hydrostatic compression up to 31 GPa. It suggests that an important issue in determining the real equilibrium phase boundary experimentally needs to be studied further.

As a result, there are two important questions for the high entropy study that needs to be answered. First, does the hydrostatic compression effectively reduce the lattice structure which could enable the various deformation modes similar to cooling? Secondly, if the answer is positive, why phase transformation from fcc to hcp is not universal in the aforementioned reports [6,17].

In this paper, we revisit the lattice-shrinkage effects by examining the *in-situ* cooling and hydrostatic compression measurements on the CoCrFeMnNi HEA. Explicitly, it is an extension of our previous reports [9,17] of temperature effects on the CoCrFeMnNi HEAs, where we investigated the temperature-dependent mechanical-behavior transitions.

2. Materials and experiments

A CoCrFeMnNi HEA (also known as Cantor alloy) was prepared with equal molar compositions with elemental powders of Co, Cr, Fe, Mn, and Ni by vacuum arc-melting. The purity of elemental powders is higher than 99.9% (in weight percent). After arc-melting, the ingot was heated to 1273 K for 6 h for homogenization and then cold rolled at room temperature with an average grain size of 100 μm. After rolling, the samples were milled into powders.

2.1. In-situ x-ray diffraction measurements

The ground powders of the CoCrFeMnNi sample were measured by X-ray diffraction method at room temperature to 12 K using the Bruker D8 Discover X-ray Diffraction System at the National Chiao Tung University. The CoCrFeMnNi samples were compressed using a symmetric diamond anvil cell (DAC), which is the hydrostatic compression test method as previously reported [18]. Pressure was measured using the ruby fluorescence technique [19]. *In-situ* Angle-dispersive X-ray diffraction (ADXRD) measurements were performed using the beamline BL01C2 at the National Synchrotron Radiation Research Center (NSRRC) and beamline BL13-BM-C at Advanced Photon Source (APS) of Argonne National Laboratory (ANL). The wavelengths were 0.435 Å (28.5 keV) and 0.434 Å (28.5 keV) for BL01C2 and BL13-BM-C, respectively. Neon was used as a pressure-transmitting medium at those beamlines to reduce the deviatoric stress in the sample during compression. The procedures of *in-situ* diffraction experiments are similar to Lin et al.'s [18] measurement.

Diffraction peaks were integrated into one dimension from the two-dimensional detector by using GSAS-II software. A least square Gaussian fitting method was used to analyze the integrated diffraction peak with single-peak fitting function. Based on the diffraction peak positions, the elastic lattice strains (ε) are calculated using the equation: $\varepsilon = (d - d_o)/d_o$, where the d_o is the stress-free interplanar spacing at room temperature, d is the interplanar spacings subjected to either stressed or different temperature conditions.

3. Results

Fig. 1(a) and (b) show the (1 1 1) and (2 0 0) lattice strain curves measured during the hydrostatic compression tests (blue circles) and cooling (red squares) of the CoCrFeMnNi HEA, respectively. It can be noted that the hydrostatic compression reduces the lattice spacings of
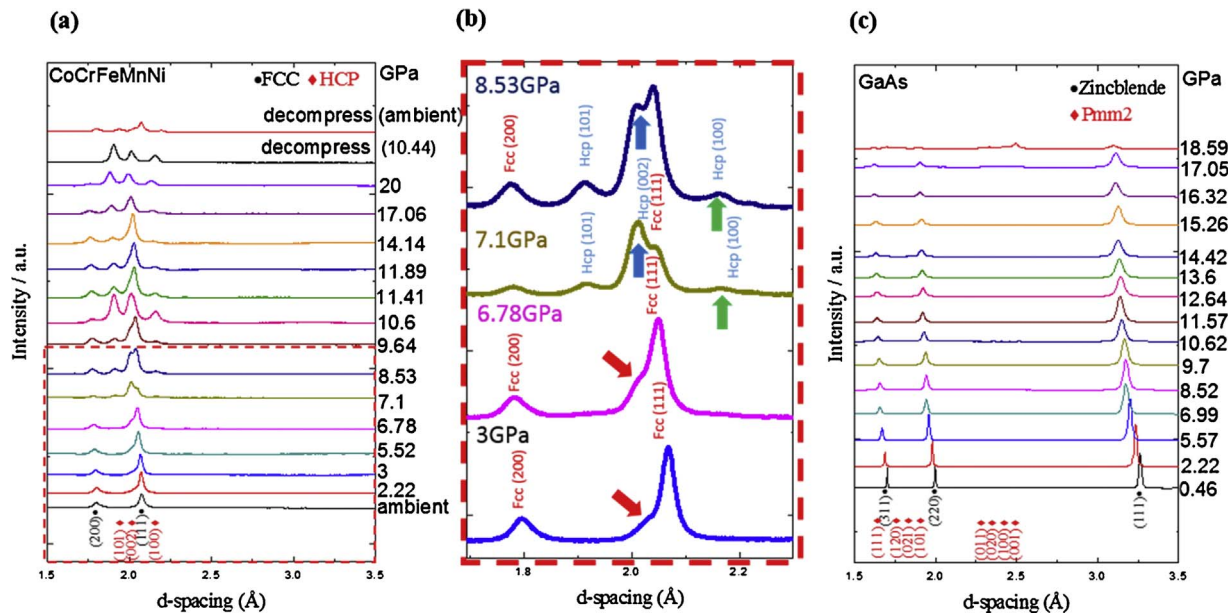
Fig. 2. Integrated diffraction-profile evolutions under hydrostatic compression for CoCrFeMnNi HEA: (a) from ambient pressure up to 20 GPa and decompressed to 10 GPa and ambient conditions. (b) Highlight the 3–8.5 GPa of (a). (c) Integrated diffraction-profile evolutions subjected to hydrostatic compression for a n-type GaAs:Si.

(1 1 1) and *(2 0 0)*. When the hydrostatic compression exceeds 2.53 GPa, the applied stress compresses the lattice strain of *(2 0 0)* to about 2930 $\mu\varepsilon$, similar to the cooling effect down to 15 K, which also makes the lattice strain of *(2 0 0)* to cold shrink to about 2900 $\mu\varepsilon$. Upon compression, the *(1 1 1)* and *(2 0 0)* diffraction peaks of fcc shifted to high angles, which demonstrates the compression of HEA lattices.

To check whether there is a phase transformation from fcc to hcp in this sample, the diffraction profiles measured by *in-situ* high-pressure synchrotron x-ray have been analyzed as shown in Fig. 2(a). The diffraction patterns of the alloys displayed in Fig. 2(a) are from ambient pressure to about 20 GPa. From the ambient pressure up to around 7 GPa, we observed mainly *(1 1 1)* and *(2 0 0)* of the fcc phase. The emerging of *(0 0 2)* and *(1 0 1)* of the hcp phase were observed in the diffraction profiles when the applied stress was up to 7.1 GPa, which is the onset of phase transformation from fcc to hcp phase. Both the phases coexist in the applied stress of 7.1–9.8 GPa. The *(1 0 0)*, *(0 0 2)*, and *(1 0 1)* of the hcp phase start to dominate the diffraction profiles from 10.28 GPa up to 20 GPa, the maximum hydrostatic compression of our experiments. The samples were then relaxed with unloading up to 10.44 GPa. Moreover, the samples were unloaded to the ambient conditions and relaxed for 24 h for the final measurement as seen in the top of Fig. 2(a) in red. Our pressure-quenched pattern reveals that the hcp phase of CoCrFeMnNi HEAs can be partially retainable, agreeing well with recently published reports [13,14].

To highlight the changes from 3 to 8.5 GPa, four selected diffraction profiles are presented in Fig. 2(b). The diffraction profiles of the CoCrFeMnNi HEAs under high pressure up to around 7 GPa are mainly *(1 1 1)* and *(2 0 0)* peaks of the fcc structure as indexed in Fig. 2(b) in red. From the systematic shifts of the diffraction peaks *(1 1 1)*, the skew of the diffraction profile, as indicated by red arrows, suggests the possibility of stacking faults formation related to the phase transformation. As can be obtained in principle, the shifts of these reflections, in the case of the present specimen, have been compared with respect to the undeformed condition [20]. There is formation of the hcp phase as the *(0 0 2)* and *(1 0 0)* peaks as indexed by blue and green arrows, respectively.

From Fig. 2(a) and (b), the results exhibit that there are stacking faults formation accompanied with the fcc to hcp phase transformation. To verify the validity of our testing methods, the same experimental setup was applied on the n-type silicon-doped gallium arsenide

(GaAs:Si) powders. The details of the experiments are archived elsewhere [18]. The experiments on the n-type GaAs:Si were performed up to 18.6 GPa. The phase transformation in the n-type GaAs:Si has occurred in between 16.4 and 18.6 GPa.

Our results also revealed the coexistence of both the fcc and the hcp phase during the wide range of the applied stress, which is in agreement with Zhang et al.'s [13–15] observations of the sluggish phase transformation for HEAs. Moreover, Lin et al. [18] reported that there is pressure-induced dislocation activities in the n-type GaAs:Si. For further comparison, the peak-width evolutions of both the n-type GaAs:Si and the CoCrFeMnNi systems are shown in Fig. 3(a) and (b), respectively.

4. Discussion

There are various microstructure effects which can cause peak broadening [21–24]. It is also not trivial to resolve the peak profiles of the overlapped fcc and hcp peaks subjected to deformation in the intermediate stages. In this study, we focus on the peak-width evolution before the phase transformation. For the n-type GaAs:Si, the peak-width evolution at the full width of the half maximum (FWHM) is compared below 16 GPa (Fig. 3a). Similarly, for the CoCrFeMnNi HEA, the peak-width evolutions of the fcc before the formation of hcp are shown in Fig. 3(b).

The FWHM of *(1 1 1)*, *(2 2 0)*, and *(3 1 1)* of the n-type GaAs:Si at ambient temperature subjected to hydrostatic compression are described in black squares, red circles, and blue triangles, respectively (Fig. 3a). The peak broadening for all the *(1 1 1)*, *(2 2 0)*, and *(3 1 1)* peaks subjected to the compression can be noticed in Fig. 3(a). In Fig. 3(b), the y-axis of the FWHM is in the same scale as depicted in Fig. 3(a) for the comparison. However, unlike the profound peak broadenings for the n-type GaAs:Si, the FWHM of the CoCrFeMnNi HEA does not increase significantly at the same level. The inset of Fig. 3(b) shows the FWHM evolutions in a smaller range for detail. Certainly, upon hydrostatic compression, there is also significant peak broadening for the CoCrFeMnNi HEA. However, when compared the peak-width broadening within 7 GPa of both samples, all peaks of the n-type GaAs:Si broaden more significantly than those of CoCrFeMnNi HEA.

The gallium arsenide (GaAs) is one of the most studied III–V compound semiconductors. It is reported that gallium has an
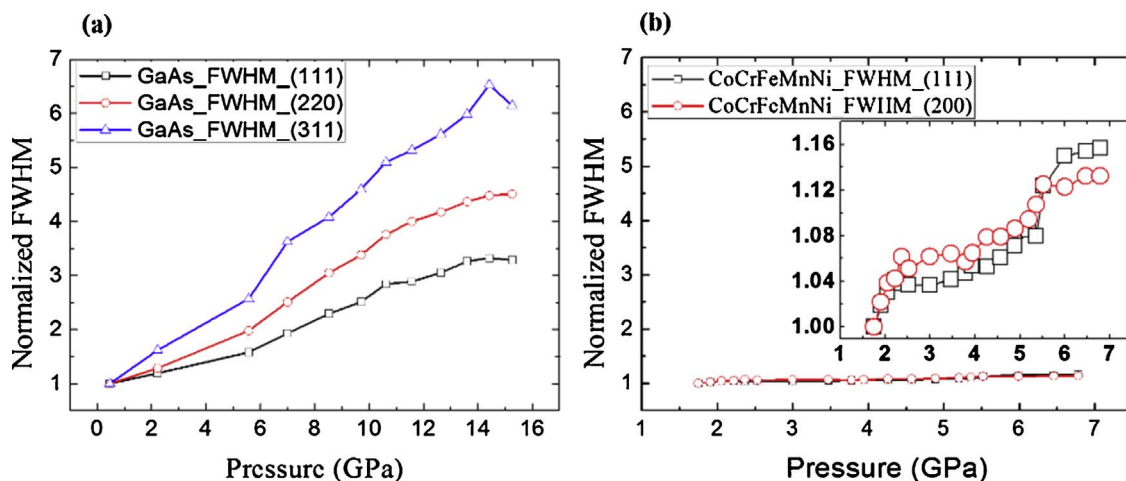
Fig. 3. Peak-width evolution in full widths at the half maximum for (a) a n-type GaAs:Si: (1 1 1) as black squares; (2 2 0) as red circles, and (3 1 1) as blue triangles; (b) for CoCrFeMnNi HEA: (1 1 1) as black squares and (2 0 0) as red circles.

electronegativity of 1.81 and arsenic has 2.18 on the Pauling scale. The small difference leads to an almost covalent bond [25]. It is clearly not the case for the CoCrFeMnNi HEA as the majority of the CoCrFeMnNi HEA bond is metallic.

Metallic bonding in the form of an electron cloud of delocalized electrons is known for the sharing of free electrons among lattices. On the other hand, the covalent bonds involve the sharing of a pair of valence electrons between two atoms. For the n-type silicon-doped gallium arsenide (GaAs:Si), Si tends to occupy Ga site as the dopant. Consequently, the GaAs:Si crystals resulted in n-type GaAs [26]. The nature of the metallic bonds allows the CoCrFeMnNi HEA to accommodate the deformation and applied stresses with less lattice distortion. The metallic bonds of HEA may also allow the rearrangements of the lattice, such as stacking fault, easily when the samples are subjected to deformation [3,27].

In the present investigation, the onset of the phase transformation can be observed at 7.1 GPa. It should be noted that the onset of phase-transformation stress in our CoCrFeMnNi HEA is lower than that of CoCrFeNiPd, which is 74 GPa [15], CoCrNi, which is 34.4 GPa [3], CoCrFeNi, which is 13.5 GPa [15], and Cr-6Fe-21Ni-9Mn, which is 12.8 GPa [28]. Moreover, if we compare the possibility of the phase transformation of the principal elements of the CoCrFeMnNi HEAs, it is reported that Co has phase transformation from hcp to fcc at 105 GPa [29]; Cr requires 10 GPa for structural transitions [30]; Fe starts fcc-hcp phase transformation at 13 GPa [31,32]; Mn is stable up to 165 GPa [33], and there is no phase transitions observed up to 260 GPa for Ni [34]. In summary, the mixing of different elements which is the major effect of the HEAs may enhance the possibility for phase transformation.

Finally, to examine the stability of the phase transformation of our CrCrFeMnNi HEA, the samples were decompressed for 24 h in ambient condition. Next, the diffraction data were collected again with the same setup. The ambient-pressure data of both the initial and relaxed states shown at the bottom and on the top of Fig. 2(a), respectively, was enlarged in Fig. 4. The differences between initial (black line) and relaxed (red line) states are depicted in blue dashes in Fig. 4. The differences and the profiles of the relaxed states reveal that there is mixture of fcc and hcp phases after 24 h relaxation. The results may agree with previous reports [5,13,14] that there might be negative stacking faults energy for the HEAs, indicating the complex microstructure is the nature of the HEAs.

5. Conclusion

In this paper, the lattice-shrinkage effects in the CoCrFeMnNi HEA
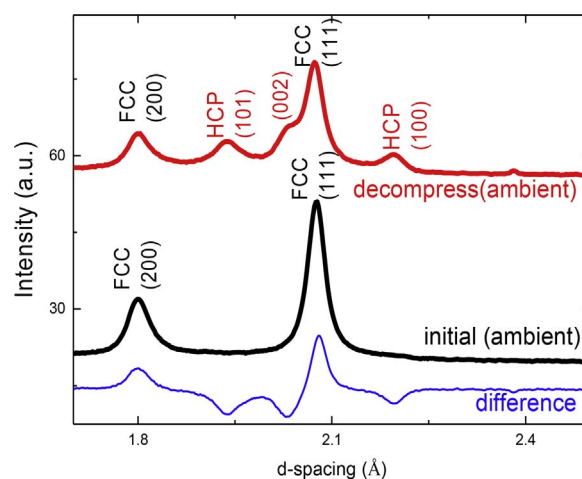
Fig. 4. X-ray diffraction profile of CoCrFeMnNi HEA before hydrostatic compression (black line) and after decompression from 20 GPa to ambient for 24 h (red line). The difference is shown in blue dashed line. The lattice planes of fcc and hcp phases are indexed in black and red *(hkl)*, respectively.

have been studied under cooling and hydrostatic compression. During hydrostatic compression, the lattice structure can be reduced as cooling the HEAs. Our results suggested that there are much stronger deformation-induced peak broadening in the n-type GaAs:Si than that of the CoCrFeMnNi HEAs. In addition, there is a microstructure evolution accompanied with the fcc to hcp phase transformation during the hydrostatic deformation in compression, which is in agreement well with recently published reports. In this study, the phase transformation in the CoCrFeMnNi HEA alloy starts at 7.1 GPa. Our study suggests that there might be size-dependent confinement for the configuration entropy, which may control the entropy effects for the phase transformation.

References

[1] B. Gludovatz, A. Hohenwarter, D. Catoor, E.H. Chang, E.P. George, R.O. Ritchie, A fracture-resistant high-entropy alloy for cryogenic applications, Science 345 (6201) (2014) 1153–1158.

[2] B. Gludovatz, A. Hohenwarter, K.V.S. Thurston, H. Bei, Z. Wu, E.P. George, et al., Exceptional damage-tolerance of a medium-entropy alloy CrCoNi at cryogenic temperatures, Nat. Commun. 7 (2016) 10602.

[3] S. Huang, W. Li, S. Lu, F. Tian, J. Shen, E. Holmström, et al., Temperature dependent stacking fault energy of FeCrCoNiMn high entropy alloy, Scr. Mater. 108 (2015) 44–47.

[4] Z. Zhang, H. Sheng, Z. Wang, B. Gludovatz, Z. Zhang, E.P. George, et al., Dislocation mechanisms and 3D twin architectures generate exceptional strength-ductility-toughness combination in CrCoNi medium-entropy alloy, Nat. Commun. 8 (2017) 14390.

[5] Y.H. Zhang, Y. Zhuang, A. Hu, J.J. Kai, C.T. Liu, The origin of negative stacking fault energies and nano-twin formation in face-centered cubic high entropy alloys, Scr. Mater. 130 (2017) 96–99.

[6] P.F. Yu, L.J. Zhang, H. Cheng, H. Zhang, M.Z. Ma, Y.C. Li, et al., The high-entropy alloys with high hardness and soft magnetic property prepared by mechanical alloying and high-pressure sintering, Intermetallics 70 (2016) 82–87.

[7] Y. Wu, W.H. Liu, X.L. Wang, D. Ma, A.D. Stoica, T.G. Nieh, et al., In-situ neutron diffraction study of deformation behavior of a multi-component high-entropy alloy, Appl. Phys. Lett. 104 (5) (2014) 051910.

[8] F. Otto, A. Dlouhý, C. Somsen, H. Bei, G. Eggeler, E.P. George, The influences of temperature and microstructure on the tensile properties of a CoCrFeMnNi high-entropy alloy, Acta Mater. 61 (15) (2013) 5743–5755.

[9] E.-W. Huang, D. Yu, J.-W. Yeh, C. Lee, K. An, S.-Y. Tu, A study of lattice elasticity from low entropy metals to medium and high entropy alloys, Scr. Mater. 101 (2015) 32–35.

[10] D.B. Miracle, O.N. Senkov, A critical review of high entropy alloys and related concepts, Acta Mater. 122 (2017) 448–511.

[11] Duancheng Ma, Blazej Grabowski, Fritz Körmann, Jörg Neugebauer, Dierk Raabe, Ab initio thermodynamics of the CoCrFeMnNi high entropy alloy: importance of entropy contributions beyond the configurational one, Acta Mater. 100 (2015) 90–97.

[12] Fuyang Tian, Lajos Károly Varga, Jiang Shen, Levente Vitos, Calculating elastic constants in high-entropy alloys using the coherent potential approximation: current issues and errors, Comput. Mater. Sci 111 (2016) 350–358.

[13] F. Zhang, Y. Wu, H. Lou, Z. Zeng, V.B. Prakapenka, E. Greenberg, et al., Polymorphism in a high-entropy alloy, Nat. Commun. 8 (2017) 15687.

[14] Cameron L. Tracy, S. Park, Dylan R. Rittman, Steven J. Zinkle, Hongbin Bei, Maik Lang, Rodney C. Ewing, Wendy L. Mao, High pressure synthesis of a hexagonal close-packed phase of the high-entropy alloy CrMnFeCoNi, Nat. Commun. 8 (2017) 15634 1–6.

[15] F. Zhang, S. Zhao, K. Jin, H. Bei, D. Popov, C. Park, et al., Pressure-induced fcc to hcp phase transition in Ni-based high entropy solid solution alloys, Appl. Phys. Lett. 110 (1) (2017) 011902.

[16] P. Yu, L. Zhang, J. Ning, M. Ma, X. Zhang, Y. Li, et al., Pressure-induced phase transitions in HoDyYGdTb high-entropy alloy, Mater. Lett. 196 (2017) 137–140.

[17] W. Woo, E.-W. Huang, J.-W. Yeh, H. Choo, C. Lee, S.-Y. Tu, In-situ neutron diffraction studies on high-temperature deformation behavior in a CoCrFeMnNi high entropy alloy, Intermetallics 62 (2015) 1–6.

[18] K.-L. Lin, C.-M. Lin, Y.-S. Lin, S.-R. Jian, Y.-F. Liao, Y.-C. Chuang, et al., Structural properties of pressure-induced structural phase transition of Si-doped GaAs by angular-dispersive X-ray diffraction, Appl. Phys. A 122 (2) (2016) 1–6.

[19] H. Mao, J.-A. Xu, P. Bell, Calibration of the ruby pressure gauge to 800 kbar under quasi-hydrostatic conditions, J. Geophys. Res.: Solid Earth 91 (B5) (1986) 4673–4676.

[20] T. Ungár, S. Ott, P.G. Sanders, A. Borbély, J.R. Weertman, Dislocations: grain size and planar faults in nanostructured copper determined by high resolution X-ray diffraction and a new procedure of peak profile analysis, Acta Mater. 46 (10) (1998) 3693–3699.

[21] E.-W. Huang, J. Qiao, B. Winiarski, W.-J. Lee, M. Scheel, C.-P. Chuang, et al., Microyielding of core-shell crystal dendrites in a bulk-metallic-glass matrix composite, Sci. Rep. 4 (2014) 4394.

[22] E.-W. Huang, R.I. Barabash, B. Clausen, Y.-L. Liu, J.-J. Kai, G.E. Ice, et al., Fatigue-induced reversible/irreversible structural-transformations in a Ni-based superalloy, Int. J. Plast. 26 (8) (2010) 1124–1137.

[23] E.-W. Huang, R.I. Barabash, G.E. Ice, W. Liu, Y.-L. Liu, J.-J. Kai, et al., Cyclic-loading-induced accumulation of geometrically necessary dislocations near grain boundaries in an Ni-based superalloy, Jom 61 (12) (2009) 53.

[24] E.-W. Huang, R. Barabash, N. Jia, Y.-D. Wang, G.E. Ice, B. Clausen, et al., Slip-system-related dislocation study from in-situ neutron measurements, Metall. Mater. Trans. A 39 (13) (2008) 3079.

[25] J.M. Zuo, J.C.H. Spence, M. O'Keeffe, Bonding in GaAs, Phys. Rev. Lett. 61 (3) (1988) 353–356.

[26] B. Cordero, V. Gómez, A.E. Platero-Prats, M. Revés, J. Echeverría, E. Cremades, et al., Covalent radii revisited, Dalton Trans. 21 (2008) 2832–2838.

[27] B.S. Murty, J.W. Yeh, S. Ranganathan, High Entropy Alloys, Elsevier Science & Technology, 2014.

[28] L. Liu, Q.-Y. Hou, Y. Zhang, Q.-M. Jing, Z.-G. Wang, Y. Bi, et al., Structural and magnetic transition in stainless steel Fe-21Cr-6Ni-9 Mn up to 250 GPa, Chin. Phys. B 24 (6) (2015) 066103.

[29] C.S. Yoo, H. Cynn, P. Söderlind, V. Iota, New beta(fcc)-Cobalt to 210 GPa, Phys. Rev. Lett. 84 (18) (2000) 4132–4135.

[30] L.C. Ming, M.H. Manghnani, Isothermal compression of bcc transition metals to 100 kbar, J. Appl. Phys. 49 (1) (1978) 208–212.

[31] J.C. Jamieson, A. Lawson, X-Ray diffraction studies in the 100 kilobar pressure range, J. Appl. Phys. 33 (3) (1962) 776–780.

[32] T. Takahashi, W.A. Bassett, High-pressure polymorph of iron, Science 145 (3631) (1964) 483–486.

[33] H. Fujihisa, K. Takemura, Stability and the equation of state of α-manganese under ultrahigh pressure, Phys. Rev. B 52 (18) (1995) 13257.

[34] I. Sergueev, L. Dubrovinsky, M. Ekholm, O.Y. Vekilova, A. Chumakov, M. Zając, et al., Hyperfine splitting and room-temperature ferromagnetism of Ni at multimegabar pressure, Phys. Rev. Lett. 111 (15) (2013) 157601.